

Phonon-assisted control of magnonic and electronic band splitting

Subhadeep Bandyopadhyay,^{1,2} Anoop Raj,³ Philippe Ghosez,¹ Sumiran Pujari,³ and Sayantika Bhowal^{3,*}

¹*Theoretical Materials Physics, Q-MAT, Université de Liège, B-4000 Sart-Tilman, Belgium*

²*Consiglio Nazionale delle Ricerche (CNR-SPIN), Unità di Ricerca presso Terzo di Chieti, c/o Università G. D'Annunzio, I-66100 Chieti, Italy*

³*Department of Physics, Indian Institute of Technology Bombay, Mumbai 400076, India*

(Dated: December 9, 2024)

We demonstrate theoretically the ability to control non-relativistic magnonic and electronic spin splitting by manipulating phonon modes. Using MnF_2 as a representative material, exhibiting non-relativistic spin splitting in its electronic bands, we identify an equivalent d -wave splitting in magnon modes of specific handedness. Our study reveals a direct correlation between magnonic and electronic splittings, showing that the energy splitting in both magnon and electronic bands can be tuned by jointly modulating the A_{2u} and A_{1g} phonon modes with frequencies of 8.52 and 9.74 THz, respectively. These findings highlight the intricate interplay between charge, spin, and lattice degrees of freedom in spin-split antiferromagnets, offering new pathways for phonon-driven control in magnonic applications.

Manipulating magnetism through optically excited structural distortions has emerged as a promising avenue in the field of ultrafast magnetism and spintronics [1]. Optical excitation can generate transient structural distortions in materials, such as lattice vibrations or phonon modes, which, in turn, alter the magnetic interactions between atoms. This allows control over magnetic phases, the switching of magnetic order, and even ultrafast demagnetization [2–6]. These effects not only offer new avenues for light-driven magnetism control but also deepen our understanding of the intricate coupling between lattice, charge, and spin degrees of freedom. Such dynamic control of magnetism on ultra-fast timescales is crucial for the development of future high-speed magnetic devices [7].

In this work, we demonstrate phonon-assisted (with frequencies in the THz regime) control of spin splitting in both electronic and magnonic bands of MnF_2 , a representative spin-split antiferromagnet (SSAFM), also known as “altermagnet”. SSAFMs are distinguished by significant spin splitting in momentum space, even without spin-orbit coupling (SOC) or net magnetization [8–24]. By combining traits of ferromagnets and conventional antiferromagnets (AFMs), SSAFMs offer new possibilities for achieving otherwise difficult properties, such as efficient spin-current generation [25–29], spin-splitting torque [30, 31], giant magnetoresistance [32], spontaneous Hall effect [21, 33–39] without any magnetization; unconventional superconducting properties [40–45], and enhanced thermal transport [46, 47], etc.

Recent theoretical proposals [48, 49], now confirmed by inelastic neutron scattering experiments [50], suggest that magnon bands in SSAFMs exhibit similar splitting to electronic bands, resulting in non-degenerate magnon modes with specific handedness—referred to as chiral magnons [48]. This development brings us closer to re-

alizing advanced magnonic devices that rely on magnon-generated spin currents in AFMs, functioning without the need for external magnetic fields to generate spin splitting [51].

In this work, we use MnF_2 as a representative material for SSAFMs. Our interest in MnF_2 stems from recent discoveries in this nearly century-old material [52–54], which highlight unusual spin splitting [9], the presence of ferroic ordering of higher-order magnetic octupoles [55, 56], and ongoing efforts [57–60] to manipulate its magnetism via structural modifications. Our key findings are threefold: First, we demonstrate that the magnon bands in MnF_2 exhibit a d -wave splitting, similar to its electronic bands. We identify that at the wave vector where this splitting is maximized, the magnon bands possess a pure handedness, which is crucial for detection using polarized neutron or X-ray scattering techniques. Second, we identify two stable Γ -point phonon modes in MnF_2 and show that by jointly controlling these modes, it is possible to manipulate the energy splitting between the magnon bands. Third, we reveal a striking correlation between electronic and magnonic bands, enabling phonon-assisted control of spin splitting in the electronic bands as well.

Our work advances the current understanding of the interplay between structural geometry and magnetism in SSAFMs. We go beyond symmetry considerations to show that the local geometry of nonmagnetic atoms plays a crucial role in inducing anisotropic magnetization density in the ground state, leading to direction-dependent exchange coupling between magnetic atoms. While the anisotropic magnetization density, characterized by ferroic magnetic octupoles [55], is essential for spin splitting in electronic bands, we analytically demonstrate that magnon band splitting arises from the direction-dependent exchange coupling. Thus, by tuning the positions of nonmagnetic atoms via specific phonon modes, we can simultaneously control both electronic and magnonic spin splittings. The proposed phonon-assisted control offers a route for ultrafast manipulation of advanced magnonic devices.

* sbhowal@iitb.ac.in

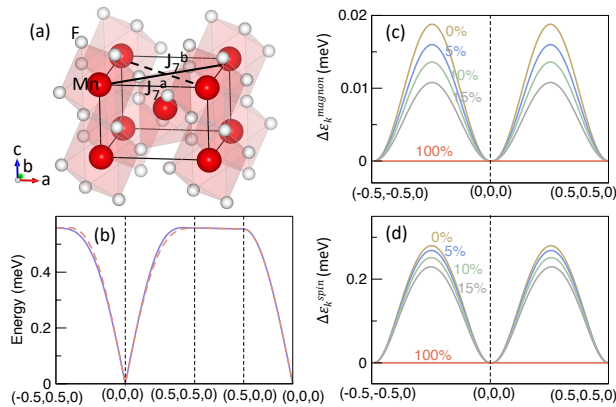


FIG. 1. Control of magnon and electronic spin splitting in MnF_2 by tuning the ground state A_{2u} and A_{1g} phonon modes. (a) Crystal structure of MnF_2 , indicating the Mn ions on the ab plane corresponding to the J_7 exchange coupling. The solid and dashed lines indicate the interactions along $[110]$ (J_7^a) and $[\bar{1}\bar{1}0]$ (J_7^b) directions with and without the F ions sitting in between respectively. (b) Computed magnon spectrum of MnF_2 . The constant term γ_k , which is identical for both branches, has been scaled by a factor of 0.1 to make the splitting more apparent. (c) The variation in magnon splitting as a function of the amplitude of phonon distortion modes, A_{2u} and A_{1g} , along specific directions in the momentum space. (d) The corresponding NRSS in the electronic band structure along the same k path for different amplitudes of the distortion.

Magnon spectra in MnF_2 - We begin by demonstrating the magnon band splitting in MnF_2 . MnF_2 crystallizes in the rutile structure ($P4_2/mnm$) (see Fig. 1a), with spin moments aligned along the $[001]$ direction and antiparallel between Mn ions [52–54]. This magnetic ordering breaks global time-reversal symmetry (\mathcal{T}), resulting in spin splitting in the ground state electronic band structure [9, 55]. To investigate whether the magnon bands exhibit a similar splitting, we first construct the relevant spin model by calculating the Heisenberg exchange interactions between Mn^{2+} ions ($S = 5/2$). These interactions are computed by mapping the total energy obtained from DFT+ U [61–64] calculations to a Heisenberg spin model for four different collinear magnetic configurations [65–67].

From the computed exchange interactions (J_i) up to the seventh nearest neighbors (NNs) ($i = 1, 7$), we find that the magnitude of the intra-sublattice coupling J_7 varies with direction ($[110]$ vs. $[\bar{1}\bar{1}0]$). This direction-dependent exchange interaction arises from the crystal geometry. As illustrated in Fig. 1a, the exchange path between the corner (central) Mn ions associated with J_7 involves F atoms along the $[110]$ ($[\bar{1}\bar{1}0]$) direction but not along $[\bar{1}\bar{1}0]$ ($[110]$). This leads to stronger coupling along the former and weaker coupling along the latter. We refer to these exchange couplings as J_7^a and J_7^b respectively. A similar direction-dependent exchange has been reported for the iso-structural compound RuO_2 [48]. However, in

MnF_2 , the magnitude of further neighbor coupling J_7 is much smaller compared to RuO_2 , likely because MnF_2 is an insulator, whereas RuO_2 is metallic.

Based on our computed exchange couplings, we construct the spin Hamiltonian relevant for MnF_2 , which is our starting point to obtain the magnon dispersion relation. Through analytical spin-wave calculations, using the Holstein-Primakoff transformation [68] and the Fourier transformation, we obtain the Hamiltonian in terms of the bosonic operators a_k and b_k in the reciprocal space as

$$H_k = \sum_k [A_k a_k^\dagger a_k + B_k b_k^\dagger b_k + C_k a_k b_{-k} + C_k^* a_k^\dagger b_{-k}^\dagger] \quad (1)$$

Here, A_k , B_k , and C_k are periodic functions of the momentum \vec{k} and have explicit dependence on J_i s (see the Supplemental Materials [67] for details). We then diagonalize the Hamiltonian using Bogoliubov transformation. The resulting Hamiltonian in terms of the magnon operators of α and β modes reads as:

$$H_k = \sum_k [\epsilon_\alpha(k) \alpha_k^\dagger \alpha_k + \epsilon_\beta(k) \beta_k^\dagger \beta_k]. \quad (2)$$

Here, $\epsilon_{\alpha,\beta}(k) = \frac{1}{2}(\pm \Delta \epsilon_k + \gamma_k)$, with $\gamma_k = [(A_k + B_k)^2 - 4C_k^2]^{1/2}$ and the energy splitting $\Delta \epsilon_k^{\text{magnon}}$ between the two magnon modes is

$$\Delta \epsilon_k^{\text{magnon}} = \epsilon_\alpha(k) - \epsilon_\beta(k) = 4(J_7^b - J_7^a) \sin(k_x a) \sin(k_y a). \quad (3)$$

This constitutes an analytical demonstration of the splitting between the magnon bands (see Fig. 1b) occurring due to the direction-dependent exchange coupling J_7 . It is also clear from Eq. (3) that $\Delta \epsilon_k^{\text{magnon}}$ switches sign under C_4 rotation of the wave vector \vec{k} , leading to the same d -wave pattern as the spin splitting in the electronic bands. We further note that the splitting $\Delta \epsilon_k^{\text{magnon}}$ is maximum at $\vec{k} \equiv (\frac{\pi}{2a}, \frac{\pi}{2a}, \frac{\pi}{a})$ at which, interestingly, the eigenvectors are $[1 \ 0]^T$ and $[0 \ 1]^T$, i.e., has a pure handedness. The splitting $\Delta \epsilon_k^{\text{magnon}}$ is small in magnitude in the case of MnF_2 of the order of $\sim 0.02 \text{meV}$. A recent *unpolarized* inelastic neutron scattering experiment with a resolution of approximately 0.1meV [69] did not detect this splitting, concluding that spin splitting is absent. This highlights the need for techniques such as polarized neutrons or circularly polarized photons, which are sensitive to the handedness of magnons. The pure handedness at $\vec{k} \equiv (\frac{\pi}{2a}, \frac{\pi}{2a}, \frac{\pi}{a})$ may provide sufficient contrast to make this effect observable in experiments.

Phonon assisted control of magnon splitting- Since the magnon splitting $\Delta \epsilon_k^{\text{magnon}}$ originates from the inequivalent J_7 exchange couplings, $\Delta \epsilon_k^{\text{magnon}}$ can be tuned by controlling the difference $\Delta J_7 = (J_7^b - J_7^a)$. Furthermore, since ΔJ_7 results from the inequivalent F environment around the Mn ions for the different exchange paths corresponding to J_7^a and J_7^b , we can control ΔJ_7 and hence the magnon splitting by manipulating the position of the F atoms.

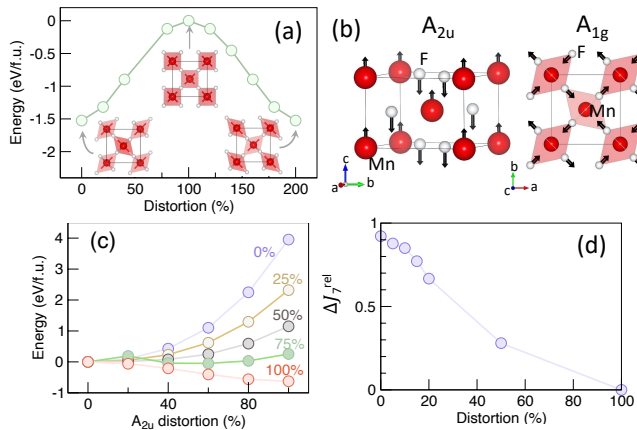


FIG. 2. (a) The variation in the total energy as a function of distortion amplitude. The 0%, 100%, and 200% distortions correspond to the actual crystal structure, the reference structure with zero spin splitting, and the opposite structural domain with opposite spin splitting. (b) Pictorial depiction of A_{2u} (left) and A_{1g} (right) phonon modes. The black arrows indicate the displacements of the Mn and F ions in the unit cell. (c) The total energy as a function of A_{2u} distortion for different amplitudes of A_{1g} distortions, showing that the structure with stronger A_{2u} distortion also energetically favors stronger A_{1g} distortion. (d) Variation of ΔJ_7^{rel} as a function of the amplitude of phonon distortion.

With this idea, we construct a higher-energy reference structure, corresponding to the space group $P4_2/nmm$, by linearly interpolating the two structural domains of MnF_2 as depicted at the inset of Fig. 2a. In this reference structure, the F atoms are shifted from the plane containing the Mn atoms such that no F atoms are present between the seventh neighbor Mn atoms, suppressing thereby ΔJ_7 .

We emphasize that our choice of the reference structure is not unique. However, it is guided by the fact that the distortion of the chosen reference structure, $P4_2/nmm$, can be represented in terms of the two stable Γ phonon modes corresponding to the A_{2u} and A_{1g} irreducible representations (IRs) of the ground state structure $P4_2/mnm$. We identify these phonon modes by explicitly carrying out the phonon calculations for the ground state $P4_2/mnm$ structure using the finite difference method as implemented within the Phonopy [70] and then projecting the distorted $P4_2/nmm$ structure on the Γ point phonon eigenvectors of the $P4_2/mnm$ structure [71–73].

We note that the polar distortion A_{2u} is infrared active [74], describing the displacements of the Mn and F atoms in the opposite direction along the c axis (see Fig. 2b) such that it lowers the symmetry of the structure to $P4_2nm$. In contrast, the A_{1g} phonon mode is isosymmetric and Raman-active. The A_{1g} phonon mode describes the displacement of the F atoms on the ab plane, as depicted in Fig. 2 b, which resembles the Q_{2z} Jahn-Teller distortion [75] of the MnF_6 octahedra. The com-

puted frequencies of the A_{2u} and A_{1g} phonon modes are, respectively, 284 cm^{-1} (8.52 THz) and 325 cm^{-1} (9.74 THz), suggesting the possibility of activating the polar A_{2u} mode using suitable infrared optical excitation.

Next, to analyze whether the joint control of the A_{2u} and A_{1g} phonon modes is energetically favorable for the system, we perform additional calculations to compute the variation in total energy as a function of the amplitude of the A_{2u} phonon modes for different amplitudes of the A_{1g} mode. The results of our calculations are depicted in Fig. 2c. It is clear from the plot that as the A_{2u} distortion increases, the minima of the total energy shifts towards larger A_{1g} distortion. This suggests that the simultaneous condensation of the A_{1g} phonon mode lowers the energy of the system and is likely to be preferred when we modulate the A_{2u} mode using infrared optical excitation. Coupling between these two modes is attributed to the symmetry allowed terms in the free energy,

$$U_{\text{coupling}} \propto Q_{A_{2u}}^2 Q_{A_{1g}} + Q_{A_{2u}}^2 Q_{A_{1g}}^2 + O(Q^5) \quad (4)$$

where Q_i is the distortion amplitude of the mode $i = A_{2u}, A_{1g}$. This coupling can potentially be activated experimentally, as demonstrated in CoF_2 [58], where trilinear coupling between two infrared-active and one Raman-active mode induces piezomagnetism.

We now proceed to show that the magnon-splitting indeed can be manipulated with the joint control of these two phonon modes. For this, we construct several intermediate structures between the ground state structure $P4_2/mnm$ and the reference structure $P4_2/nmm$ by jointly varying the two phonon modes. We compute the variation of the exchange interactions across the intermediate structures. The resulting change ΔJ_7^{rel} in the seventh NN coupling, $\Delta J_7^{\text{rel}} = \left| \frac{\Delta J_7}{(J_7^a + J_7^b)} \right|$, is shown in Fig. 2a. As we see from the plot, ΔJ_7^{rel} gradually decreases with an increase in the distortion and eventually vanishes at the reference structure $P4_2/nmm$ (See Fig. 2d). Consequently, we can tune the magnon splitting $\Delta \varepsilon_k^{\text{magnon}}$ by controlling the phonon-modes, as depicted in Fig. 1c. We note that with increasing distortion, J_2 and J_5 exchange couplings also gradually become inequivalent [67]. However, both being inter-sublattice coupling, do not contribute to the splitting of the magnon bands [67].

Connection to spin splitting in the electronic bands- To investigate the impact of controlling jointly the phonon modes A_{2u} and A_{1g} on the electronic bands, we further analyze the corresponding electronic bands for intermediate distortions. The results are shown in Fig. 1c. As evident from the figure, the spin splitting between electronic bands decreases with increasing distortion and, eventually, vanishes for the reference structure, similar to what we observe with the magnon bands. This indicates a correlation between the splitting in the electronic and magnonic bands.

To explore the origin of the connection between electronic and magnonic bands, we compute the band-decomposed magnetization density for structures with

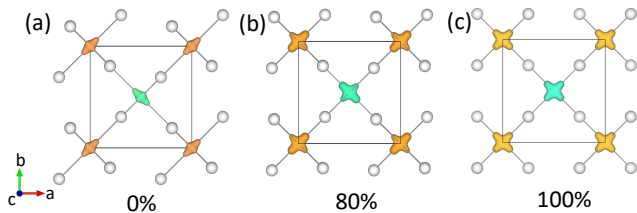


FIG. 3. The computed magnetization densities for three different distortion amplitudes (a) 0%, (b) 80%, and (c) 100%. The isosurface value is set to 0.1 for all the plots. Different colors of the magnetization density denote the opposite spin polarization around the corner and center Mn ions. The white balls represent the F atoms.

0%, 80%, and 100% distortions. Here, 0% corresponds to the ground-state structure, while 100% refers to the reference structure. As seen in Figs. 3 a-c, the anisotropy in the magnetization density decreases with increasing distortion. For 0% distortion, the magnetization density around the Mn ions is highly anisotropic, taking on an elliptical shape, with the long axis aligned along the Mn-Mn bond corresponding to the seventh neighbor, with two F atoms between them. This anisotropic magnetization is linked to the direction-dependent J_7 exchange coupling as the larger magnetization density implies a stronger interaction along that particular Mn-Mn bond.

Interestingly, this same anisotropic magnetization density, described by the magnetic octupole, has previously been shown to play a key role in the spin splitting of electronic bands [55]. The computed magnitude of the ferroically ordered atomic site magnetic octupole component $\mathcal{O}_{32^-} = -2.5 \times 10^{-3} \mu_B$ per Mn atom. As distortion increases, the F atoms move away from the Mn-Mn bond, and the magnetization density shifts to form two ellipsoids along the Mn-Mn bonds associated with J_7 , thus reducing ΔJ_7^{el} . At 100% distortion, the anisotropy in the magnetization density is minimized, and our multipole calculations [67, 76–78] show the absence of ferroic magnetic octupoles with $\mathcal{O}_{32^-} = 0$. Correspondingly, ΔJ_7^{el} also vanishes resulting in an absence of splitting between the magnon bands, revealing the origin of the connection between splitting in the electronic and magnonic bands.

The phonon-driven manipulation of electronic and magnonic splitting, as demonstrated in our study, is not exclusive to MnF_2 or other isostructural transition metal difluorides. This concept is general and should apply to other SSAFMs, including those exhibiting g -wave spin

splitting with anisotropic magnetization density, characterized by magnetic triakontadipoles [79] rather than magnetic octupoles. While the specific phonon modes may vary across different materials, it remains feasible to control the positioning of nonmagnetic atoms by carefully analyzing the relevant phonon modes, thus enabling the regulation of splitting in both magnon and electronic bands.

To summarize, our work uncovers the intricate correlation between phonons, electrons, and magnons in SSAFMs, by explicitly demonstrating the control of the dispersion relation for the last two by tuning the former. The proposed phonon-assisted manipulation of the magnon and electronic splitting may be probed using time-resolved magneto-optical Kerr measurements and time-resolved resonant inelastic scattering measurements. Interestingly, a recent study highlights the coupling between magnons and infrared-active polar phonons via the dynamic modulation of magnetic exchange interactions in CoF_2 , demonstrated using far-infrared and dielectric spectroscopy techniques [74]. This finding provides a promising experimental framework to validate the coupling mechanism we propose for MnF_2 . We hope that our work will open up a new paradigm for ultra-fast manipulation of SSAFMs, motivating future research along these directions.

ACKNOWLEDGEMENTS

We thank Abhishek Nag, Urs Staub, and Nicola A. Spaldin for stimulating discussions. SBa acknowledges use of the CECI supercomputer facilities funded by the F.R.S-FNRS (Grant No. 2.5020.1) and of the Tier-1 supercomputer of the Fédération Wallonie-Bruxelles funded by the Walloon Region (Grant No. 1117545). AR acknowledges the financial support provided by CSIR-HRDG, India, in the form of a Senior Research Fellowship (SRF). SP acknowledges financial support from SERB, DST, Govt. of India (Grant No. MTR/2022/000386). SBh thanks National Supercomputing Mission for providing computing resources of ‘PARAM Porul’ at NIT Trichy, implemented by C-DAC and supported by the Ministry of Electronics and Information Technology (MeitY) and Department of Science and Technology, Government of India and acknowledges funding support from the Industrial Research and Consultancy Centre (IRCC) Seed Grant (RD/0523-IRCCSH0-018) and the INSPIRE research grant (project code RD/0124-DST0030-002).

-
- [1] A. Kirilyuk, A. V. Kimel, and T. Rasing, Ultrafast optical manipulation of magnetic order, *Rev. Mod. Phys.* **82**, 2731 (2010).
 [2] E. Beaurepaire, J.-C. Merle, A. Daunois, and J.-Y. Bigot, Ultrafast spin dynamics in ferromagnetic nickel, *Phys.*

- Rev. Lett.* **76**, 4250 (1996).
 [3] A. V. Kimel, A. Kirilyuk, A. Tsvetkov, R. V. Pisarev, and T. Rasing, Laser-induced ultrafast spin reorientation in the antiferromagnet tmfeo_3 , *Nature* **429**, 850 (2004).

- [4] I. Radu, K. Vahaplar, C. Stamm, T. Kachel, N. Pontius, H. A. Dürr, T. A. Ostler, J. Barker, R. F. L. Evans, R. W. Chantrell, A. Tsukamoto, A. Itoh, A. Kirilyuk, T. Rasing, and A. V. Kimel, Transient ferromagnetic-like state mediating ultrafast reversal of antiferromagnetically coupled spins, *Nature* **472**, 205 (2011).
- [5] D. M. Juraschek, M. Fechner, A. V. Balatsky, and N. A. Spaldin, Dynamical multiferroicity, *Phys. Rev. Mater.* **1**, 014401 (2017).
- [6] M. Basini, M. Pancaldi, B. Wehinger, M. Udina, V. Unikandanunni, T. Tadano, M. C. Hoffmann, A. V. Balatsky, and S. Bonetti, Terahertz electric-field-driven dynamical multiferroicity in SrTiO_3 , *Nature* **628**, 534 (2024).
- [7] T. Zalewski, A. Maziewski, A. V. Kimel, and A. Stupakiewicz, Ultrafast all-optical toggle writing of magnetic bits without relying on heat, *Nature Communications* **15**, 4451 (2024).
- [8] S. Hayami, Y. Yanagi, and H. Kusunose, Momentum-dependent spin splitting by collinear antiferromagnetic ordering, *J. Phys. Soc. Jpn.* **88**, 123702 (2019).
- [9] L.-D. Yuan, Z. Wang, J.-W. Luo, E. I. Rashba, and A. Zunger, Giant momentum-dependent spin splitting in centrosymmetric low- z antiferromagnets, *Phys. Rev. B* **102**, 014422 (2020).
- [10] L.-D. Yuan, Z. Wang, J.-W. Luo, and A. Zunger, Prediction of low- z collinear and noncollinear antiferromagnetic compounds having momentum-dependent spin splitting even without spin-orbit coupling, *Phys. Rev. Materials* **5**, 014409 (2021).
- [11] L. Šmejkal, J. Sinova, and T. Jungwirth, Beyond conventional ferromagnetism and antiferromagnetism: A phase with nonrelativistic spin and crystal rotation symmetry, *Phys. Rev. X* **12**, 031042 (2022).
- [12] L.-D. Yuan and A. Zunger, Degeneracy removal of spin bands in collinear antiferromagnets with non-interconvertible spin-structure motif pair, *Advanced Materials* **35**, 2211966 (2023).
- [13] Y. Guo, H. Liu, O. Janson, I. C. Fulga, J. van den Brink, and J. I. Facio, Spin-split collinear antiferromagnets: A large-scale ab-initio study, *Mater. Today Phys.* **32**, 100991 (2023).
- [14] S. Zeng and Y.-J. Zhao, Description of two-dimensional altermagnetism: Categorization using spin group theory, *Phys. Rev. B* **110**, 054406 (2024).
- [15] S. Lee, S. Lee, S. Jung, J. Jung, D. Kim, Y. Lee, B. Seok, J. Kim, B. G. Park, L. Šmejkal, C.-J. Kang, and C. Kim, Broken Kramers degeneracy in altermagnetic MnTe, *Phys. Rev. Lett.* **132**, 036702 (2024).
- [16] J. Krempaský, L. Šmejkal, S. W. D'Souza, M. Hajaoui, G. Springholz, K. Uhlířová, F. Alarab, P. C. Constantinou, V. Strocov, D. Usanov, W. R. Pudelko, R. González-Hernández, A. Birk Hellenes, Z. Jansa, H. Reichlová, Z. Šobáň, R. D. Gonzalez Betancourt, P. Wadley, J. Sinova, D. Krieger, J. Minár, J. H. Dil, and T. Jungwirth, Altermagnetic lifting of Kramers spin degeneracy, *Nature* **626**, 517 (2024).
- [17] S. Reimers, L. Odenbreit, L. Šmejkal, V. N. Strocov, P. Constantinou, A. B. Hellenes, R. Jaeschke Ubierno, W. H. Campos, V. K. Bharadwaj, A. Chakraborty, T. Denneulin, W. Shi, R. E. Dunin-Borkowski, S. Das, M. Kläui, J. Sinova, and M. Jourdan, Direct observation of altermagnetic band splitting in CrSb thin films, *Nat Commun* **15**, 2116 (2024).
- [18] T. Aoyama and K. Ohgushi, Piezomagnetic properties in altermagnetic mntes, *Phys. Rev. Mater.* **8**, L041402 (2024).
- [19] Z. Lin, D. Chen, W. Lu, X. Liang, S. Feng, K. Yamagami, J. Osiecki, M. Leandersson, B. Thiagarajan, J. Liu, C. Felser, and J. Ma, Observation of giant spin splitting and d-wave spin texture in room temperature altermagnet RuO_2 (2024), arXiv:2402.04995 [cond-mat.mtrl-sci].
- [20] K.-H. Ahn, A. Hariki, K.-W. Lee, and J. Kuneš, Antiferromagnetism in RuO_2 as d -wave Pomeranchuk instability, *Phys. Rev. B* **99**, 184432 (2019).
- [21] L. Šmejkal, R. González-Hernández, T. Jungwirth, and J. Sinova, Crystal time-reversal symmetry breaking and spontaneous hall effect in collinear antiferromagnets, *Sci. Adv.* **6**, eaaz8809 (2020), <https://www.science.org/doi/pdf/10.1126/sciadv.aaz8809>.
- [22] L. Šmejkal, J. Sinova, and T. Jungwirth, Emerging research landscape of altermagnetism, *Phys. Rev. X* **12**, 040501 (2022).
- [23] P. A. McClarty and J. G. Rau, Landau theory of altermagnetism, *Phys. Rev. Lett.* **132**, 176702 (2024).
- [24] L. Bai, W. Feng, S. Liu, L. Šmejkal, Y. Mokrousov, and Y. Yao, Altermagnetism: Exploring new frontiers in magnetism and spintronics (2024), arXiv:2406.02123 [cond-mat.mtrl-sci].
- [25] M. Naka, S. Hayami, H. Kusunose, Y. Yanagi, Y. Motome, and H. Seo, Spin current generation in organic antiferromagnets, *Nat. Commun.* **10**, 4305 (2019).
- [26] R. González-Hernández, L. Šmejkal, K. Výborný, Y. Yahagi, J. Sinova, T. Jungwirth, and J. Železný, Efficient electrical spin splitter based on nonrelativistic collinear antiferromagnetism, *Phys. Rev. Lett.* **126**, 127701 (2021).
- [27] D.-F. Shao, S.-H. Zhang, M. Li, C.-B. Eom, and E. Y. Tsybal, Spin-neutral currents for spintronics, *Nat. Commun.* **12**, 7061 (2021).
- [28] A. Bose, N. J. Schreiber, R. Jain, D.-F. Shao, H. P. Nair, J. Sun, X. S. Zhang, D. A. Muller, E. Y. Tsybal, D. G. Schlom, and D. C. Ralph, Tilted spin current generated by the collinear antiferromagnet ruthenium dioxide, *Nat. Electron.* **5**, 267 (2022).
- [29] M. Hu, O. Janson, C. Felser, P. McClarty, J. van den Brink, and M. G. Vergniory, Spin hall and edelstein effects in novel chiral noncollinear altermagnets (2024), arXiv:2410.17993 [cond-mat.mtrl-sci].
- [30] H. Bai, L. Han, X. Y. Feng, Y. J. Zhou, R. X. Su, Q. Wang, L. Y. Liao, W. X. Zhu, X. Z. Chen, F. Pan, X. L. Fan, and C. Song, Observation of spin splitting torque in a collinear antiferromagnet RuO_2 , *Phys. Rev. Lett.* **128**, 197202 (2022).
- [31] S. Karube, T. Tanaka, D. Sugawara, N. Kadoguchi, M. Kohda, and J. Nitta, Observation of spin-splitter torque in collinear antiferromagnetic RuO_2 , *Phys. Rev. Lett.* **129**, 137201 (2022).
- [32] L. Šmejkal, A. B. Hellenes, R. González-Hernández, J. Sinova, and T. Jungwirth, Giant and tunneling magnetoresistance in unconventional collinear antiferromagnets with nonrelativistic spin-momentum coupling, *Phys. Rev. X* **12**, 011028 (2022).
- [33] L. Šmejkal, A. H. MacDonald, J. Sinova, S. Nakatsuji, and T. Jungwirth, Anomalous hall antiferromagnets, *Nature Reviews Materials* **7**, 482 (2022).
- [34] H. Reichlová, R. L. Seeger, R. González-Hernández, I. Kounta, R. Schlitz, D. Krieger, P. Ritzinger, M. Lam-

- mel, M. Leiviskä, V. Petříček, P. Doležal, E. Schmoranzarová, A. Bad'ura, A. Thomas, V. Baltz, L. Michez, J. Sinova, S. T. B. Goennenwein, T. Jungwirth, and L. Šmejkal, Macroscopic time reversal symmetry breaking by staggered spin-momentum interaction, arXiv 2012.15651 10.48550/ARXIV.2012.15651 (2020).
- [35] Z. Feng, X. Zhou, L. Šmejkal, L. Wu, Z. Zhu, H. Guo, R. González-Hernández, X. Wang, H. Yan, P. Qin, X. Zhang, H. Wu, H. Chen, Z. Meng, L. Liu, Z. Xia, J. Sinova, T. Jungwirth, and Z. Liu, An anomalous hall effect in altermagnetic ruthenium dioxide, *Nat. Electron.* **5**, 735 (2022).
- [36] R. D. Gonzalez Betancourt, J. Zubáč, R. Gonzalez-Hernandez, K. Geishendorf, Z. Šobán, G. Springholz, K. Olejnik, L. Šmejkal, J. Sinova, T. Jungwirth, S. T. B. Goennenwein, A. Thomas, H. Reichlová, J. Železný, and D. Krieger, Spontaneous anomalous hall effect arising from an unconventional compensated magnetic phase in a semiconductor, *Phys. Rev. Lett.* **130**, 036702 (2023).
- [37] L. Šmejkal, A. H. MacDonald, J. Sinova, S. Nakatsuji, and T. Jungwirth, Anomalous hall antiferromagnets, *Nat. Rev. Mater.* **7**, 482 (2022).
- [38] S.-W. Cheong and F.-T. Huang, Altermagnetism with non-collinear spins, *npj Quantum Materials* **9**, 13 (2024).
- [39] T. Sato, S. Haddad, I. C. Fulga, F. F. Assaad, and J. van den Brink, Altermagnetic anomalous hall effect emerging from electronic correlations, *Phys. Rev. Lett.* **133**, 086503 (2024).
- [40] I. I. Mazin, Notes on altermagnetism and superconductivity, arXiv 2203.05000 10.48550/ARXIV.2203.05000 (2022).
- [41] D. Zhu, Z.-Y. Zhuang, Z. Wu, and Z. Yan, Topological superconductivity in two-dimensional altermagnetic metals, *Phys. Rev. B* **108**, 184505 (2023).
- [42] S. Banerjee and M. S. Scheurer, Altermagnetic superconducting diode effect, *Phys. Rev. B* **110**, 024503 (2024).
- [43] D. Chakraborty and A. M. Black-Schaffer, Zero-field finite-momentum and field-induced superconductivity in altermagnets, *Phys. Rev. B* **110**, L060508 (2024).
- [44] S.-B. Zhang, L.-H. Hu, and T. Neupert, Finite-momentum cooper pairing in proximitized altermagnets, *Nature Communications* **15**, 1801 (2024).
- [45] S. H. Lee, Y. Qian, and B.-J. Yang, Fermi surface spin texture and topological superconductivity in spin-orbit free noncollinear antiferromagnets, *Phys. Rev. Lett.* **132**, 196602 (2024).
- [46] X. Zhou, W. Feng, R.-W. Zhang, L. Šmejkal, J. Sinova, Y. Mokrousov, and Y. Yao, Crystal thermal transport in altermagnetic RuO_2 , *Phys. Rev. Lett.* **132**, 056701 (2024).
- [47] K. V. Yershov, V. P. Kravchuk, M. Daghofer, and J. van den Brink, Fluctuation-induced piezomagnetism in local moment altermagnets, *Phys. Rev. B* **110**, 144421 (2024).
- [48] L. Šmejkal, A. Marmodoro, K.-H. Ahn, R. González-Hernández, I. Turek, S. Mankovsky, H. Ebert, S. W. D'Souza, O. c. v. Šipr, J. Sinova, and T. c. v. Jungwirth, Chiral magnons in altermagnetic RuO_2 , *Phys. Rev. Lett.* **131**, 256703 (2023).
- [49] P. A. McClarty, A. Gukasov, and J. G. Rau, Observing altermagnetism using polarized neutrons (2024), arXiv:2410.10771 [cond-mat.str-el].
- [50] Z. Liu, M. Ozeki, S. Asai, S. Itoh, and T. Masuda, Chiral-split magnon in altermagnetic MnTe (2024), arXiv:2408.16490 [cond-mat.str-el].
- [51] Q. Cui, B. Zeng, P. Cui, T. Yu, and H. Yang, Efficient spin seebeck and spin nernst effects of magnons in altermagnets, *Phys. Rev. B* **108**, L180401 (2023).
- [52] W. de Haas, B. Schultz, and J. Koolhaas, Further measurements of the magnetic properties of some salts of the iron group at low temperatures, *Physica* **7**, 57 (1940).
- [53] M. S. Seehra and R. E. Helmick, Anomalous changes in the dielectric constants of MnF_2 near its néel temperature, *J. Appl. Phys.* **55**, 2330 (1984).
- [54] Z. Yamani, Z. Tun, and D. H. Ryan, Neutron scattering study of the classical antiferromagnet MnF_2 : a perfect hands-on neutron scattering teaching course, *Can. J. Phys.* **88**, 771 (2010).
- [55] S. Bhowal and N. A. Spaldin, Ferroically ordered magnetic octupoles in d -wave altermagnets, *Phys. Rev. X* **14**, 011019 (2024).
- [56] M. Costa and P. Brown, Magnetisation density in MnF_2 , *Physica B: Condensed Matter* **156-157**, 329 (1989).
- [57] E. A. Mashkovich, K. A. Grishunin, R. M. Dubrovin, A. K. Zvezdin, R. V. Pisarev, and A. V. Kimel, Terahertz light-driven coupling of antiferromagnetic spins to lattice, *Science* **374**, 1608 (2021), <https://www.science.org/doi/pdf/10.1126/science.abk1121>.
- [58] A. S. Disa, M. Fechner, T. F. Nova, B. Liu, M. Först, D. Prabhakaran, P. G. Radaelli, and A. Cavalleri, Polarizing an antiferromagnet by optical engineering of the crystal field, *Nat. Phys.* **16**, 937 (2020).
- [59] T. W. J. Metzger, K. A. Grishunin, C. Reinhofer, R. M. Dubrovin, A. Arshad, I. Ilyakov, T. V. A. G. de Oliveira, A. Ponomaryov, J.-C. Deinert, S. Kovalev, R. V. Pisarev, M. I. Katsnelson, B. A. Ivanov, P. H. M. van Loosdrecht, A. V. Kimel, and E. A. Mashkovich, Magnon-phonon fermi resonance in antiferromagnetic CoF_2 , *Nature Communications* **15**, 5472 (2024).
- [60] R. M. Dubrovin, A. Tellez-Mora, A. C. Garcia-Castro, N. V. Siverin, N. N. Novikova, K. N. Boldyrev, E. A. Mashkovich, A. H. Romero, and R. V. Pisarev, Polar phonons and magnetic excitations in the antiferromagnet CoF_2 , *Phys. Rev. B* **109**, 224312 (2024).
- [61] P. E. Blöchl, Projector augmented-wave method, *Phys. Rev. B* **50**, 17953 (1994).
- [62] G. Kresse and D. Joubert, From ultrasoft pseudopotentials to the projector augmented-wave method, *Phys. Rev. B* **59**, 1758 (1999).
- [63] G. Kresse and J. Hafner, Ab initio molecular dynamics for liquid metals, *Phys. Rev. B* **47**, 558 (1993).
- [64] G. Kresse and J. Furthmüller, Efficient iterative schemes for ab initio total-energy calculations using a plane-wave basis set, *Phys. Rev. B* **54**, 11169 (1996).
- [65] H. J. Xiang, E. J. Kan, S.-H. Wei, M.-H. Whangbo, and X. G. Gong, Predicting the spin-lattice order of frustrated systems from first principles, *Phys. Rev. B* **84**, 224429 (2011).
- [66] D. Šabani, C. Bacaksiz, and M. V. Milošević, Ab initio methodology for magnetic exchange parameters: Generic four-state energy mapping onto a heisenberg spin hamiltonian, *Phys. Rev. B* **102**, 014457 (2020).
- [67] Supplemental materials for the computational details of the dft and the magnon calculations, and the additional results for the exchange coupling calculations.
- [68] T. Holstein and H. Primakoff, Field dependence of the intrinsic domain magnetization of a ferromagnet, *Phys. Rev.* **58**, 1098 (1940).

- [69] V. C. Morano, Z. Maesen, S. E. Nikitin, J. Lass, D. G. Mazzone, and O. Zaharko, Absence of altermagnetic magnon band splitting in mnf_2 (2024), arXiv:2412.03545 [cond-mat.str-el].
- [70] A. Togo and I. Tanaka, First principles phonon calculations in materials science, *Scripta Materialia* **108**, 1 (2015).
- [71] Agate: an abinit graphical analysis tool engine, <https://github.com/abinit/agate>.
- [72] H. T. Stokes, D. M. Hatch, and B. J. Campbell, ISOTROPY Software Suite .
- [73] B. J. Campbell, H. T. Stokes, D. E. Tanner, and D. M. Hatch, *ISODISPLACE*: a web-based tool for exploring structural distortions, *Journal of Applied Crystallography* **39**, 607 (2006).
- [74] R. M. Dubrovin, A. Tellez-Mora, A. C. Garcia-Castro, N. V. Siverin, N. N. Novikova, K. N. Boldyrev, E. A. Mashkovich, A. H. Romero, and R. V. Pisarev, Polar phonons and magnetic excitations in the antiferromagnet cof_2 , *Phys. Rev. B* **109**, 224312 (2024).
- [75] S. Bandyopadhyay and P. Ghosez, Structurally triggered orbital and charge orderings in tlmno_3 and related compounds (2024).
- [76] F. Cricchio, *Multipoles in Correlated Electron Materials*, Ph.D. thesis, Uppsala University (2010).
- [77] O. Grånäs, *Theoretical Studies of Magnetism and Electron Correlation in Solids*, Ph.D. thesis, Uppsala University (2012).
- [78] N. A. Spaldin, M. Fechner, E. Bousquet, A. Balatsky, and L. Nordström, Monopole-based formalism for the diagonal magnetoelectric response, *Phys. Rev. B* **88**, 094429 (2013).
- [79] X. H. Verbeek, D. Voderholzer, S. Schären, Y. Gachnang, N. A. Spaldin, and S. Bhowal, Nonrelativistic ferromagnetotriakontadipolar order and spin splitting in hematite, *Phys. Rev. Res.* **6**, 043157 (2024).

Supplementary Material for Phonon-assisted control of magnonic and electronic band splitting

I. COMPUTATIONAL DETAILS

The electronic structure of MnF_2 , as presented in the manuscript, is computed using the plane-wave based projector augmented wave (PAW) [61, 62] method as implemented in the Vienna ab initio simulation package (VASP) [63, 64]. All the calculations are performed using the LDA+ U formalism with $U_{\text{eff}} = 5$ eV at the Mn site [9]. To achieve self-consistency, we use an energy cut-off of 550 eV and a $10 \times 10 \times 14$ k-point sampling of the Brillouin zone. The PAW potentials Mn-pv ($[\text{Mg}]3p^63d^54s^2$) and F ($[\text{He}]2s^22p^5$) are employed in the calculations. All the calculations are performed using the relaxed structure of MnF_2 . The atomic relaxations are carried out until the Hellman-Feynman forces on each atom become less than 0.005 eV/Å. The atomic-site multipoles at the

Mn ions are calculated from the decomposition of the density matrix $\rho_{lm,l'm'}$, computed within the framework of density functional theory (DFT), into the tensor moments [76–78], of which the parity even tensor moments have contributions from the $l = l'$ terms.

The exchange coupling J_i between two Mn atoms at different distances is computed using the methodology described in Refs. [65, 66]. We have calculated J_i up to the seventh nearest neighbor. To calculate the exchange coupling between two particular Mn atoms, we compute the total energy within LDA+ U for four different collinear magnetic configurations while other Mn atoms are fixed to an FM alignment. While calculating J , we used an adequate size of supercells to isolate the chosen two Mn atoms (between which the exchange coupling is to be calculated) and avoid undesired contributions from other neighbors. Accordingly, $[1 \times 1 \times 4]$, $[1 \times 1 \times 4]$, $[2 \times 2 \times 2]$, $[4 \times 2 \times 2]$, $[3 \times 3 \times 3]$, $[2 \times 2 \times 4]$, $[2 \times 2 \times 5]$, $[4 \times 4 \times 2]$ supercells are used to calculate J_i s from first to seventh neighbours respectively. As the values of J are very small, we paid special attention to reduce numerical error while calculating them. We set a tolerance of 10^{-8} eV for the energy convergence during the electronic self consistent calculations, which provided us the desired accuracy.

The phonon band structure for the ground state $P4_2/mnm$ structure of MnF_2 is computed using the finite difference method as implemented within the PHONOPY software [70]. The $P4_2/mnm$ structure of MnF_2 has six atoms in the unit cell. For the phonon band structure calculation, we considered a $2 \times 2 \times 2$ supercell, keeping the ground state antiferromagnetic spin alignment. No unstable phonon mode is found in our calculation, confirming the dynamic stability of the $P4_2/mnm$ structure. To obtain the high energy reference structure with zero spin and magnon splitting, we first construct the other structural domain with the same space group symmetry $P4_2/mnm$ but of opposite spin splitting [55]. The reference structure $P4_2/nm$ is then obtained by linearly interpolating the two structures with opposite spin splitting. The spin splitting is found to be suppressed in the reference structure $P4_2/nm$. Distortions of the $P4_2/nm$ structure can be described by the Γ point phonon modes of the ground state $P4_2/mnm$ structure, which are identified using the following two steps. First, we calculate the atomic distortions of $P4_2/nm$ relative to the $P4_2/mnm$ structure. This provides distortions in all three Cartesian directions. Next, these distortions are mapped to the phonon eigenvectors at the Γ point as given below using the AGATE software [71],

$$u_x \hat{x} + u_y \hat{y} + u_z \hat{z} = \sum_i c_i \vec{\Gamma}_i \quad (5)$$

Here, u_j with $j = x, y, z$ are the atomic distortions, and c_i s are the amplitude of the Γ point phonon i ($i = 1, \dots, 24$) mode with eigen vector $\vec{\Gamma}_i$. We find that the reference structure, $P4_2/nm$, with zero spin splitting contains distortion of the two stable Γ -phonon modes lying at 8.52

and 9.74 THz respectively with A_{2u} and A_{1g} irreducible representations. We normalize $c_{A_{2u}}$ and $c_{A_{1g}}$ to 1, which correspond to atomic distortions of 0.83\AA and 0.38\AA respectively as calculated using ISODISTORT [72, 73].

II. DETAILS OF THE MAGNON SPECTRUM IN MnF_2

In the main text, we analytically demonstrated that the direction-dependent J_7 exchange coupling is respon-

$$A_k = 2J_1 [\cos(k_z c) - 1] + 8J_2 + 2J_3 [\cos(k_y a) + \cos(k_x a) - 2] + 2J_4 [\cos(k_z c + k_x a) + \cos(k_z c - k_x a) - 2] + 2J_6 [\cos(k_z c) - 1] + 2J_7^a [\cos(k_y + k_x)a - 1] + 2J_7^b [\cos(k_y - k_x)a - 1]$$

$$B_k = 2J_1 [\cos(k_z c) - 1] + 8J_2 + 2J_3 [\cos(k_y a) + \cos(k_x a) - 2] + 2J_4 [\cos(k_z c + k_x a) + \cos(k_z c - k_x a) - 2] + 2J_6 [\cos(k_z c) - 1] + 2J_7^a [\cos(k_y - k_x)a - 1] + 2J_7^b [\cos(k_y + k_x)a - 1]$$

and

$$C_k = C_k^* = 2J_2 \left[\cos\left(\frac{k_x a + k_y a + k_z c}{2}\right) + \cos\left(\frac{k_x a + k_y a - k_z c}{2}\right) + \cos\left(\frac{k_x a - k_y a + k_z c}{2}\right) + \cos\left(\frac{-k_x a + k_y a + k_z c}{2}\right) \right].$$

Here, a and c represent the tetragonal lattice constants of the MnF_2 unit cell. J_i denotes the exchange coupling between the i^{th} nearest neighbors of Mn atoms.

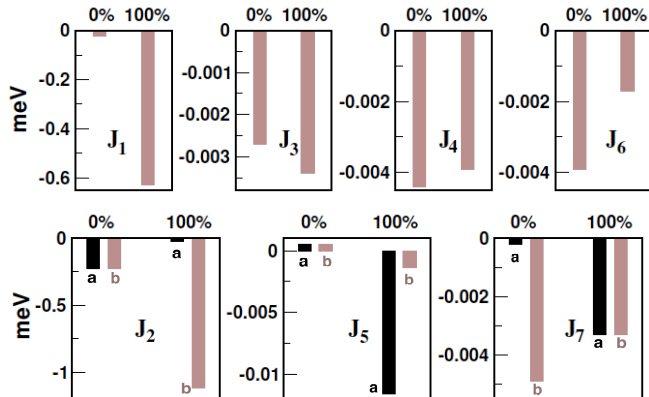


FIG. 4. Comparison of magnetic exchange interactions J_i between the $P4_2/mnm$ (0%) and $P4_2/nm$ (100%) structures.

III. ADDITIONAL RESULTS OF THE EXCHANGE COUPLINGS

The computed exchange couplings J_i up to the seventh nearest neighbor are shown in Fig. 4 as a function of distance for the ground state $P4_2/mnm$ structure and the higher energy reference structure $P4_2/nm$. As evidenced from the plot, ΔJ_7 vanishes for the reference structure, explaining the suppression of the magnon band

splitting between the magnon modes in MnF_2 , consistent with previous numerical results for the isostructural RuO_2 [48]. Here, we present the explicit forms of A_k , B_k , and C_k from Eq. (1) in the main text. These expressions are given in terms of the various exchange couplings J_i ($i = 1-7$) as follows:

splitting. We note that the J_2 and J_5 exchange couplings,

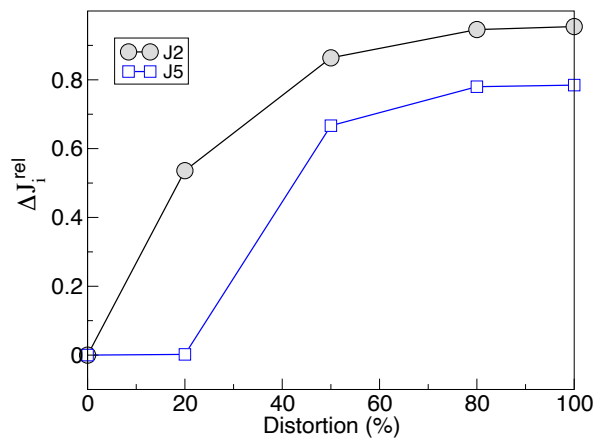


FIG. 5. The variation of ΔJ_i^{rel} for $i = 2$ and 5 as a function of amplitude of distortion.

on the other hand, become inequivalent for the reference structure. We further compute $\Delta J_i^{\text{rel}} = \left| \frac{J_i^a - J_i^b}{J_i^a + J_i^b} \right|$ for $i = 2, 5$ for intermediate structures with different amplitudes of distortion and the results are shown in Fig. 5. As discussed in the main text, ΔJ_i^{rel} however does not contribute to the splitting between magnon bands.